

OPTICAL PERFORMANCE ANALYSIS OF STANDARD MISSILE BLOCK IV A SEEKER

L. F. DeSandre
Research Department
Naval Air Warfare Center Weapons Division
China Lake, CA 93555

ABSTRACT

The flight environment of the Standard Missile, Block IV A interceptor involves high speeds that place severe aerodynamic and aero-thermal loads on the missile optical window and sensor. The supersonic flow over the missile produces aero-optical effects that can degrade IR seeker performance. This report summarizes an analysis of aero-optical aberrations due to shock front and shear layer density gradients. Computational Fluid Dynamics (CFD) models, which incorporate turbulence due to coolant spray, are used to compute the density and refractive index distribution about the IR dome. This data is then used in a ray-tracing program to determine boresite error and astigmatic lensing. These results compare favorably with computational results derived from general fluid mechanical approximations. Conclusions are drawn which indicate that boresite error may hinder seeker-targeting performance when looking in a forward direction or for low altitude intercepts.

1.0 INTRODUCTION

The performance of optical systems located in aerodynamic environments can be severely impacted. These aero-optical effects are caused by index-of-refraction variations induced by the optical platform moving through the aerodynamic flow field. Index-of-refraction variations cause an optical system (both in transmission and reception) to experience beam wander, and beam spread that results in a reduction of peak intensity and resolution. These effects should be considered in the design of airborne optical systems and performance evaluation of missile systems.

Optical aberrations resulting from aero-dynamic flow fields can be categorized as, 1) boresite error and astigmatic lensing due to shear layer laminar flow, and shear layer density gradient about the optical window, 2) turbulence in the boundary layer, 3) aero-thermal effects resulting from temperature gradients across and through the optical window.

For imaging in the infrared, a material window suffers optical transmission losses due to window radiative effects that induce background thermal noise on the detector as well as index-of-refraction variations due to temperature induce stresses within the window material. Aero-thermal effects are not considered in this report.

Flow testing data as well as window thermal analysis support the need for actively cooling the IR window. Further, cooling is indispensable for semiconductor detector materials in order to maintain in-band transmission and reduce thermal background emissions. Conceptually active cooling maintains the window at ambient temperature preserving mechanical properties such as fracture strength and hardness of window materials.

Form SF298 Citation Data

Report Date <i>("DD MON YYYY")</i> 00001999	Report Type N/A	Dates Covered (from... to) <i>("DD MON YYYY")</i>
Title and Subtitle Optical Performance Analysis of Standard Missile Block IV A Seeker		Contract or Grant Number
Authors		Program Element Number
Performing Organization Name(s) and Address(es) Research Department Naval Air Warfare Center Weapons Division China Lake, CA 93555		Project Number
Sponsoring/Monitoring Agency Name(s) and Address(es)		Task Number
Distribution/Availability Statement Approved for public release, distribution unlimited		Work Unit Number
Supplementary Notes		Performing Organization Number(s)
Abstract		Monitoring Agency Acronym
Subject Terms		Monitoring Agency Report Number(s)
Document Classification unclassified	Classification of SF298 unclassified	
Classification of Abstract unclassified	Limitation of Abstract unlimited	
Number of Pages 13		

There is, however, a system cost to active cooling. Uniform cooling of the optical dome is extremely difficult to achieve in practice. Computational Fluid Dynamics (CFD) results indicate that even through the effect of the coolant gas is to reduce the overall temperature of the dome, large thermal gradients develop across the dome surface, jeopardizing material integrity and inducing refractive index variations and hence optical aberrations. Further, the coolant flow, located in the dynamic flow field, becomes turbulent and the refractive index variations in the flow region result in pseudo-random aero-optical aberrations.

The goal of this report is to analyze optical aberrations to the missile seeker, which are relatively constant in nature for a specific flight profile. These include shock and shear layer effects. Aero-optical effects resulting from the turbulent boundary layer and coolant flow are stochastic and necessitate a statistical approach to the analysis, to be summarized in a separate report.

In the next section, a theoretical basis for analyzing aero-optical aberrations due to the shock and shear layers is presented by considering the refractive effects of an optical wave incident on layers of slight index-of-refraction variation. CFD computations, which incorporate turbulence due to coolant spray, are used to compute the density and refractive index distribution about the IR dome. Finally conclusions are drawn concerning the severity of aero-optical aberration, the implications for missile targeting performance and suggestions for further work.

2.0. THEORY

2.1. SHOCK WAVES

Shock waves result as a body accelerates through the atmosphere from the subsonic into the supersonic region. At supersonic velocities a shock wave develops, as discontinuities in the air properties such as density.

Due to the density discontinuity and hence index-of-refraction variations, the shock front both refracts and reflects the incoming optical radiation depending on the strength and angle of the shock front. In addition shock fronts usually cause low-order aberrations. For the case of a rapidly maneuvering body, the aero-optical induced aberrations can vary with time, typically with a temporal frequency related to the duration of the maneuver.

The relation between the density ahead of the shock front, ρ_1 , and density behind the front, ρ_2 , is given by:¹

$$\frac{\rho_2}{\rho_1} = \frac{(\gamma + 1)M_0^2 \sin^2 \theta}{(\gamma - 1)M_0^2 \sin^2 \theta + 2} \quad (1)$$

where γ is adiabatic index
 M_0 is free-stream Mach number
 θ is the shock angle at the optical axis

No analytical scaling relationships have been developed for determining shock front angle or density gradient; however, approximations have been derived based on CFD computations. The strength of the shock as measured by the density gradient across the shock increases with

¹ Landau and Lifshits, *Fluid Mechanics*, Vol. 6, pg. 331, Pergamon Press, 1959.

² National Advisory Committee for Aeronautics (NACA), Washington, DC, "Equations, Tables, and Charts for Compressible Flow" (U). Technical Report 1135, 1947.

Mach number. The angle of the shock front depends on the angle of attack, geometry of the vehicle, as well as the Mach number. Blunt bodies have shock detached and standing ahead of the body. Surfaces with sharp leading edges exhibit shock waves attached to the leading edge. Figure shows representative curves of shock wave angle as a function of the cone angle of the body.

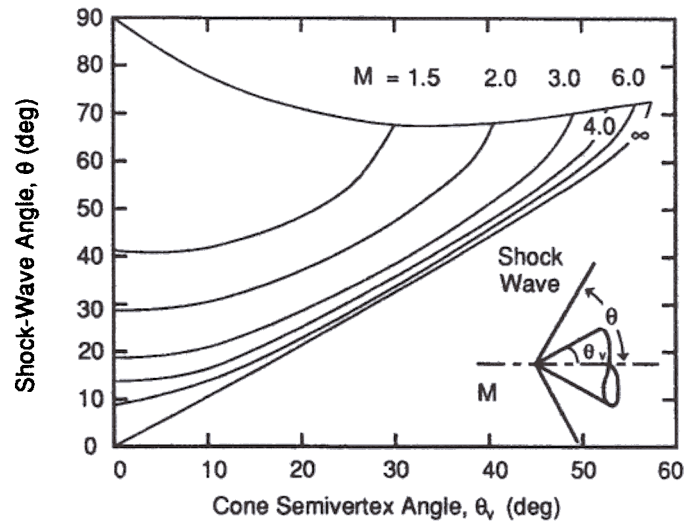


Figure 1. Shock Wave Angles.

2.2. TRACKING OR BORESITE ERROR

Density values ρ , which result from aero-dynamic analysis are related to refractive index values, n , by the Gladstone-Dale law,³ $n - 1 = G\rho$, where G is the Gladstone-Dale parameter. The Gladstone-Dale parameter is plotted in Figure 2 and can be seen to be nearly constant at $0.22 \text{ cm}^3/\text{g}$ for the wavelength $\lambda > 0.5 \text{ }\mu\text{m}$.⁴

A complex shock and flow pattern that is a unique function of the missile speed, attitude, altitude, and coolant mass flow rate is formed upstream of the dome. A shock wave is usually very stable for constant flight characteristics. Since the shock front is usually at some angle to the optical axis, an incoming light ray is refracted at the shock front interface. Using Snell's Law and the Gladstone-Dale relation, the angle of the incident ray, β_1 , is related to, β_2 , the angle of the refracted ray, both measured normal to the shock plane, by⁵

³ Philosophical transactions of the Royal Society of London. Series A, Containing papers of a mathematical or physical character. London, Royal Society of London, Vol. 148, pp. 882 or 887. G. W. Gladstone, et al., "On the Influence of Temperature on the Reflectivity of Light (U)."

⁴ Atmospheric Propagation of Light, *The Infrared and Electro-Optical Systems Handbook* (U), Vol. 2, pg. 254, ERIN, SPIE Press.

⁵ William L. Wolfe and George J. Zissis, Eds. *The Infrared Handbook* (U), The Infrared Information and Analysis (IRIA) Center, Environmental Research Institute of Michigan, 1978.

$$\sin \beta_2 = \sin \beta_1 \left(\frac{1 + G\rho_1}{1 + G\rho_2} \right) \quad (2)$$

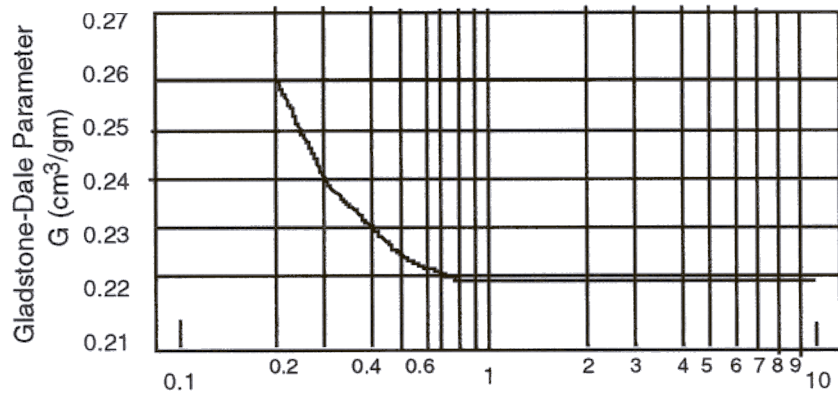


Figure 2. The Gladstone-Dale Parameter as a Function of Wavelength. Note that for $\lambda > 0.5 \mu\text{m}$, this parameter is nearly invariant ($0.22 \text{ cm}^3/\text{g}$).

2.3. FOCAL LENGTH VARIATIONS

The shock front can be represented by laminar density contours in the plane of incidence formed by the optical ray and missile axis. In the orthogonal direction the shock front is curved and acts as an aerodynamic cylindrical lens, producing astigmatism in that the sagittal ray focus behind the tangential rays. Figure 3 illustrates this case. The curved shock acts like a lens of radius equal to the distance from the vehicle center to the shock front. The effective focal length F in the plane perpendicular to the airframe longitudinal axis and at station distance x is,⁶

$$\frac{F}{x} = \left[\frac{M_1^2 \sin^2 \theta (1 + 6G\rho_1) + 5}{6G\rho_1 M_1^2 \sin^2 \theta} \right]^* \quad (3)$$

As can be seen from the above equation, the lensing effect becomes stronger with increasing Mach number and cone angle. The effect of the conical lens is to skew the focal plane, causing a defocus of the optical spot. The lens effect is actually a more complicated mechanism in that the radius of the shock depends upon the sensor look angle since the income optical ray takes a different path from the shock front to the sensor. When considered in this manner, the shock front is parabolic in shape and requires a complex integration for complete analysis. Fortunately, the focusing shift due to the curved nature of the shock front is small and the spherical shock surface approximation is adequate.

⁶ Atmospheric Propagation of Light, *The Infrared and Electro-Optical Systems Handbook (U)*, Vol. 2, pg. 252, ERIN, SPIE Press.

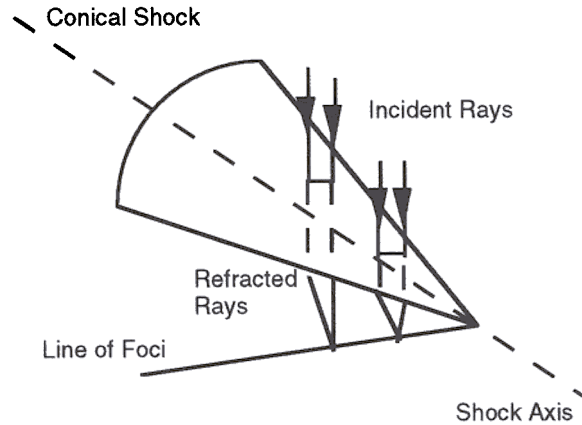


Figure 3. Shock Wave Induced Lensing Effect.

If we consider the aero-dynamic lensing of the shock front and the optical imaging system as two thin lenses then the effective focal length of the system F_e is related to the shock front focal length F and system focal length F_o , by

$$F_e = \left(\frac{1}{F} + \frac{1}{F_o} \right)^{-1} \quad (4)$$

2.3. SHEAR LAYER OPTICAL EFFECTS

The shear layer which forms from the aerodynamic flow about the optical dome also contributes to refraction and lensing of incident optical radiation. CFD computations reveal a density gradient across the shear layer typically greater than that of the shock front. Further, the shear layer is curved in the plane of incidence as the flow conforms to the hemispherical dome, producing a lensing and focal shift in the plane of incidence as well as the orthogonal plane.

The influence of the shear layer to the optical system is considered by two separate techniques. First, a computational technique, similar to that used in analyzing boresite error due to the shock front, is extended to include the shear layer. In this method, the incoming optical beam is first refracted by the shock front and intersects the shear layer. The slope and strength (density gradient) of the shear layer is determined by CFD results and depends on the optical sensor look angle. Snell's law (eg. 2) is then used to find the refractive angle through the shear layer and the overall boresite error due to refractive effects from the shock and shear layer determined.

In the second method optical effects induced by the shear layer and shock front are analyzed by employing CFD density data. Here the density contours are modeled as thin wedges of varying optical thickness and a ray tracing code used to determine the magnitude of various optical distortions. This technique is described in more detail in the following section.

2.4. RAY-TRACING FROM COMPUTATIONAL FLUID DYNAMICS

In this section, CFD models, which incorporate turbulence due to coolant spray, are used to compute the density and refractive index distribution about the IR dome including the shock, boundary, and shear layers. CFD density plot⁷ for a nominal flight profile is shown as Figure 4. This data is then used in a ray-tracing program to determine boresite error and astigmatic lensing. These results compare favorably with computational results derived from general fluid mechanical approximations reported above.

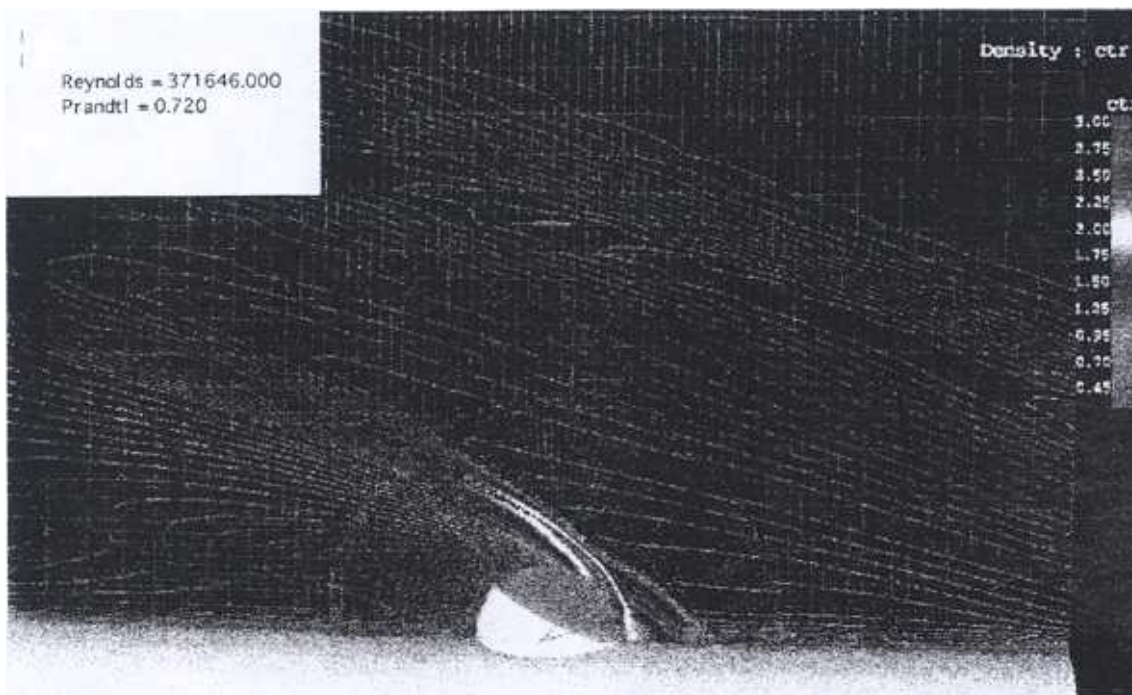


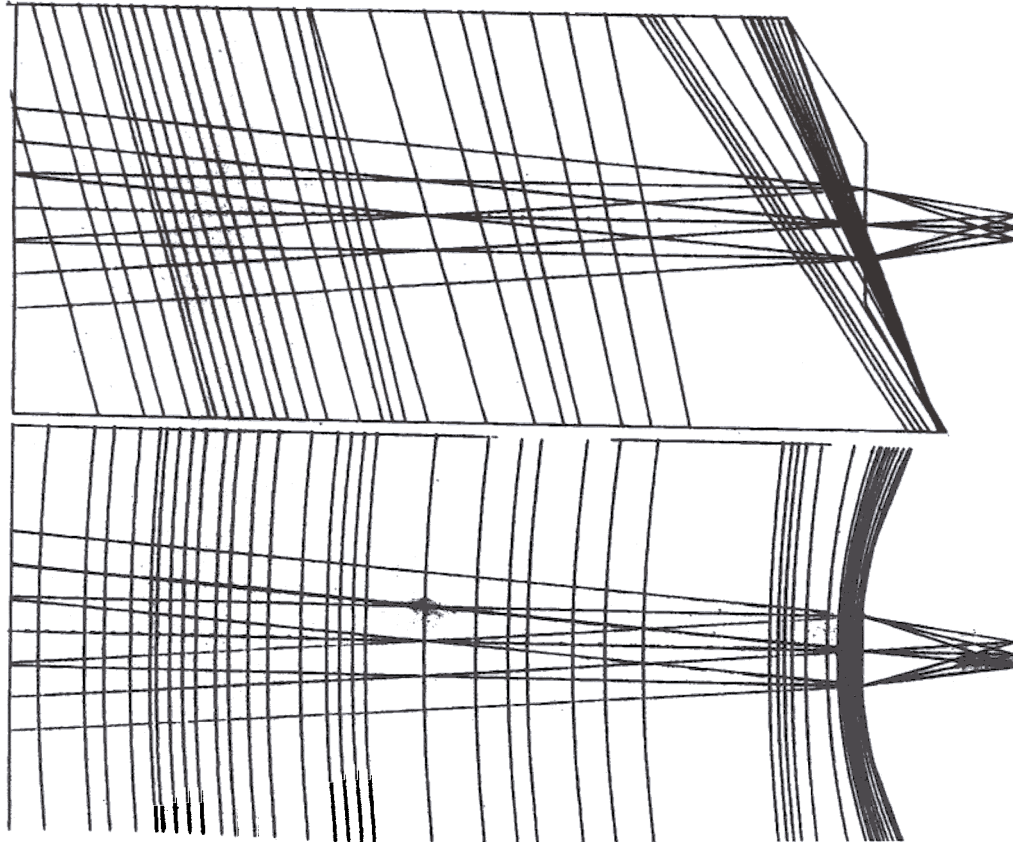
Figure 4. CFD Generated Density Contours in 0.05 kg/m^3 Steps for Nominal Flight Profile.

Ray-tracing from CFD results are briefly described for a specific look direction. The CFD density contours in steps of 0.05 kg/m^3 are converted into index-of-refraction (n) contours via the Gladstone-Dale relation. From the slope of the density contour lines with respect to the look angle, and the thickness, d , of each layer between contours, the air is modeled as thin wedges of appropriate optical thickness, nd , and tilt angle. The layers were given curvature in the orthogonal plane to model the lensing effect. The CFD density contours modeled as an optical system are illustrated in Figure 5. Index of refraction and wedge angle data are used to model the flow field in an optical ray-tracing code (ZEMAX). A 2.286-cm diameter entrance stop was placed on the window rather than at the sensor entrance pupil. A perfect lens of 5.75-cm focal length, matching the optical system of the seeker, was used in the ray-tracing routine. Three look angles were used, 0° (perpendicular to the missile longitudinal axis), 45° and 80° .

Results of the geometric ray-trace are shown as boresite error and focal spot shape, although many other performance evaluation tools are available. These techniques most clearly indicate optical degradation due to the shock and shear layer.

ZERO DEGREE LOOK ANGLE/NOMINAL FLIGHT PROFILE

Plane of Incidence



Orthogonal to Plane of Incidence

Figure 5. CFD Density Profiles Modeled as Optical Wedges of Varying Index.

3. RESULTS

The results of this paper are divided into the two sections. First, results derived from the general shock front theory are presented. This includes

- 1 Boresite error as a function of look angle for nominal flight condition.
2. Boresite error as a function of missile altitude.
3. Aerodynamic flow induced lensing.

Ray-tracing analysis from CFD generated data are shown next. This analysis includes,

- 1 Boresite error as a function of look angle for nominal flight conditions.
2. Lensing induced astigmatism.

To determine boresite error, Equation (1) was first used to calculate the density gradient across the shock front. A missile cone angle of 20° was used in Figure 1 to arrive at a 17° shock wave angle, which compares favorably to CFD results. Diffractive effects due to the shear layer were based upon density gradients determined from CFD.

Boresite error results are shown in Figures 6 and 7.

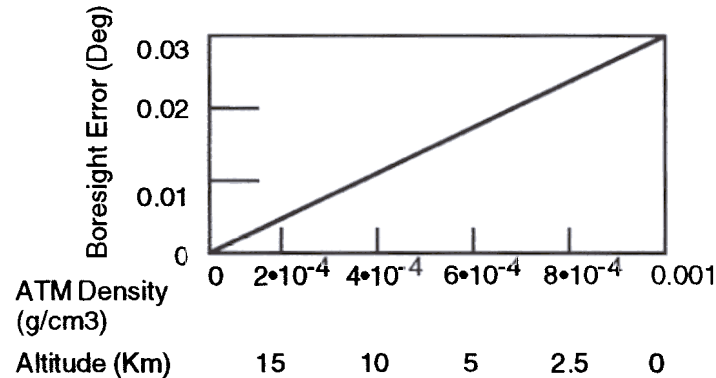


Figure 6. Boresite as a Function of Missile Attitude for Nominal Flight Profile.

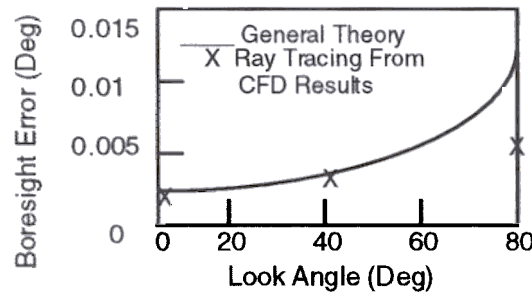


Figure 7. Boresite for Nominal Flight Profile as a Function of Look Angle Zero Degree. Angle is straight up. 90 degrees is looking forward.

Figure 6 plots boresite error for a missile traveling at Mach 4.1 at 10-degree angle of attack. The sensor look angle is 45 degrees. Boresite error is inversely proportional to the atmospheric density, since the density gradient across a shock front is directly proportional to the free stream density gradient.

Boresite error as a function of look angle for a nominal flight profile of 15-km altitude, Mach 4.1 and 10-degree angle of attack is shown in Figure 7. Results for both the general theory and ray tracing from CFD results are shown. The boresite error is quite small at small look angles but rises rapidly above 45 degrees. The focus shift for a seeker under nominal flight conditions was determined from Equations 3 and 4 and plotted in Figure 8 as a function of look angle. This calculation assumes the optical system is focusing on a target 10-km distance. As the look angle

approaches 40 degrees the focus shift effect increases rapidly, but the overall effect is still small since the astigmatic spot size is well under the diffraction limited spot.

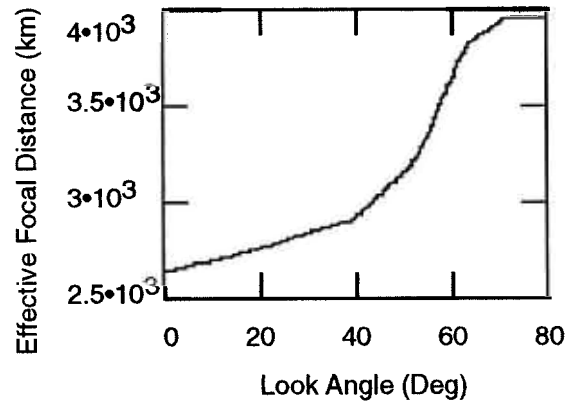


Figure 8. Effective Focal Distance as a Function of Look Angle for a Nominal Flight Profile.

Boresite error determined from ray tracing based on CFD data is also plotted in Figure 7 at three look angles. Good agreement between the general theoretical predictions and ray tracing was obtained for small look angles. Ray tracing resulted in smaller boresite error than predicted by the general theory as the look angle increased.

Spot diagrams, generated by ray tracing, are shown in Figures 9, 10, and 11 for 0, 45, and 85-degree look angles, respectively. These diagrams result from tracing numerous rays through the aero-optical system, neglecting diffraction effects, and displaying the pattern that would result on the sensor detector plane. As can be seen, a large amount of astigmatism is present in the spot diagrams, but the extent of the spot elongation is relatively small; 0.4, 1.0, and 2.0 μm for zero, 45 and 85 degree look angles, respectively. These values of lensing induced astigmatism are small compared to the Airy diffraction spot of $\text{---} \mu\text{m}$ representing the diffraction limit of the optical system with 0.9-inch entrance diameter and 2.25 inch focal length. The final diffraction pattern at the optical systems focal plane will be a convolution of the astigmatic aberrated spot and the diffraction limited airy pattern.

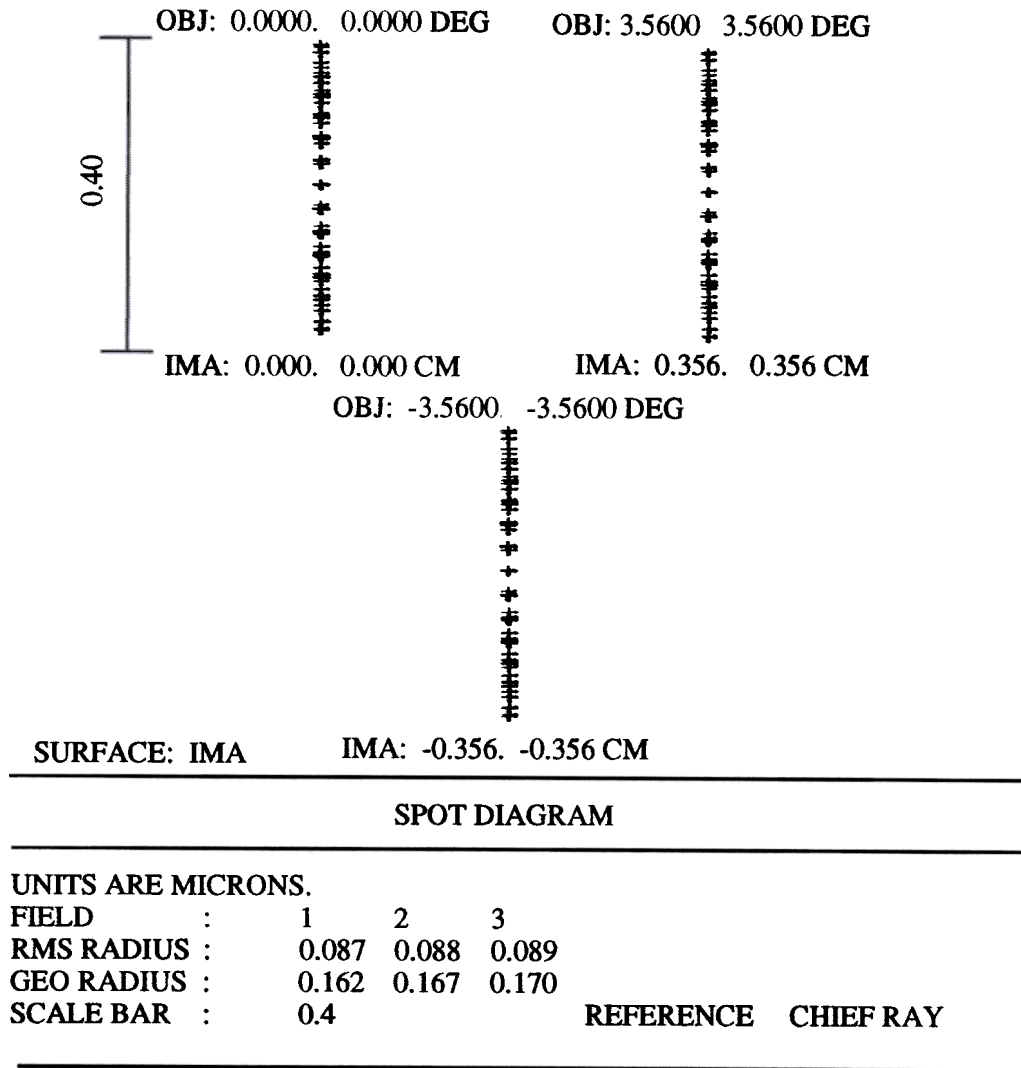


Figure 9. Zero Degree Look Angle.

OBJ: 0.0000. 0.0000 Degree OBJ: 3.5600. 3.5600 Degree



IMA: -0.000. 0.00 CM IMA: 0.356. 0.356 CM
OBJ: -3.5600. -3.5600 Degree



IMA: -0.356. -0.356 CM

SURFACE; IMA

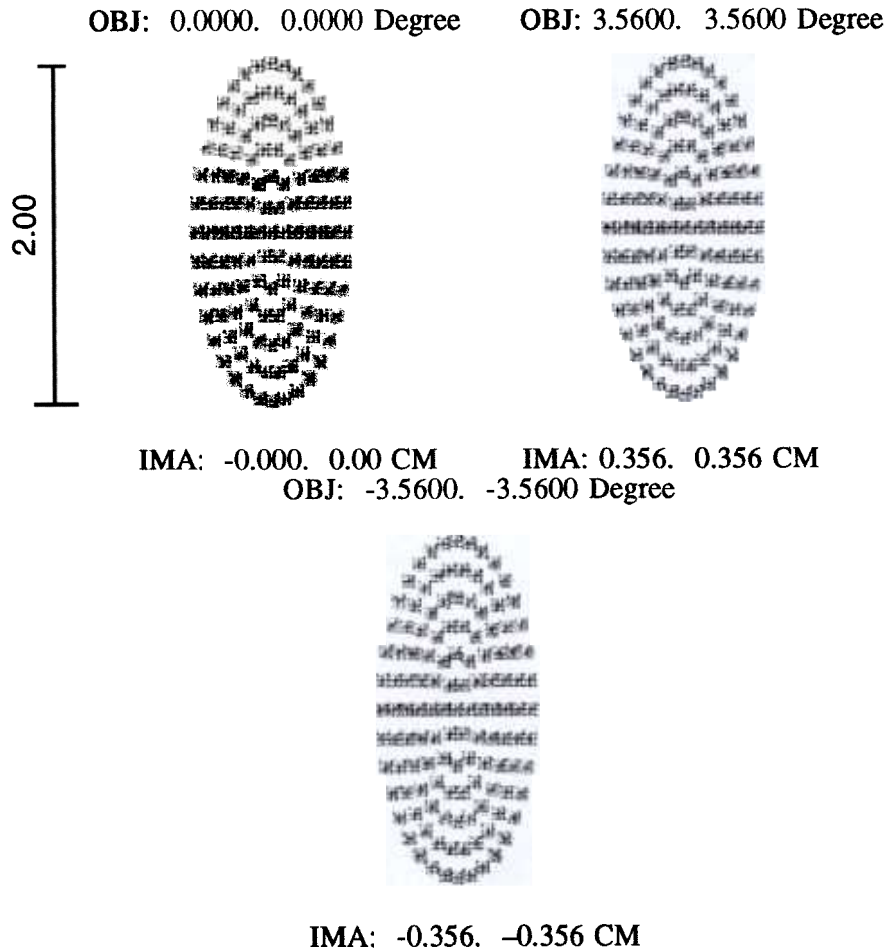
SPOT DIAGRAM

UNITS ARE MICRONS

FIELD	:	1	2	3
RMS RADIUS	:	0.342	0.347	0.345
GEO RADIUS	:	0.537	0.564	0.558
SCALE BAR	:	2		

REFERENCE : CHIEF RAY

Figure 10. 45 Degree Look Angle.



SURFACE; IMA

SPOT DIAGRAM

UNITS ARE MICRONS

FIELD	: 1	2	3
RMS RADIUS	: 0.450	0.454	0.456
GEO RADIUS	: 0.764	0.791	0.793
SCALE BAR	: 2	REFERENCE : CHIEF RAY	

Figure 11 85 Degrees Look Angle.

3.1 OPTICAL REFLECTION LOSS

Light interacting with the laminar shock front is both refracted on transmission and reflected. The reflected component, R, for unpolarized light is given by

$$R = \left(\frac{n - n_0}{n + n_0} \right)^2$$

From the Gladstone-Dale relations and assuming $n_0 = 1$, the reflectance, R , is;

$$R = \left(\frac{G\rho}{G\rho + 2} \right)^2$$

The reflectance is on the order for 10^{-9} for all look angles and is therefore considered negligible.

4. CONCLUSIONS

This report summarizes the analysis of aerodynamic induced optical distortions to the Standard Missile Block IV A interceptor.

Interaction of the flow field with the airborne platform and sensor window can induce a variety of optical effects. Density gradients in the shock front and shear layer about the hemispherical window, boundary layer turbulence, window emissivity and temperature/stress gradients result in optical aberrations, which potentially jeopardize missile tracking and targeting performance. This report considers aberrations resulting from the shock and shear layer density only. Optical effects due to random aerodynamic turbulence and aero-thermal induced aberrations are reported separately.

The analysis undertaken in support of this project was two-fold, first a theoretical approach based upon general fluid mechanical theory and second, CFD models, which incorporate turbulence due to coolant spray used in a ray tracing program to determine boresight error and astigmatic lensing. These results compare favorably with computational results derived from general fluid mechanical approximations.

Specific conclusions follow:

1. Line-of-sight (boresight errors) are small for a Mach 4.1 interceptor at 15 km altitude and zero degree (up) sensor look angle. This is equivalent to 30-cm error at 10-km target range.
2. As the look-angle increases, however, boresight becomes more severe, approaching 2 meters at 10-km distance and 78° look-angle.
3. Boresight error also decreases with increasing altitude, as expected. This has implications for interception at low altitudes. Boresight error for a target 10-km distance and 2.5-km intercept altitude is estimated at 4 meters.
4. Lensing induced astigmatism is negligible, generally much smaller than the diffraction limited spot.
5. Reflection loss at the shock interface is negligible.